Structural Organization of Photosynthetic Apparatus in Agranal Chloroplasts of Maize[*]

Elzbieta Romanowska[‡1], **Joanna Kargul**[§], **Marta Powikrowska**[‡], **Giovanni Finazzi**[¶], **Jon Nield**[||2], **Anna Drozak**[‡], **and Berenika Pokorska**[‡]

From the [‡]*Department of Plant Physiology, University of Warsaw, Miecznikowa 1, 02-096 Warsaw, Poland,* [§]*Division of Molecular Biosciences, Faculty of Natural Sciences, Imperial College London, London SW7 2AZ, United Kingdom, the* [||]*School of Biological and Chemical Sciences, Queen Mary, University of London, Mile End Road, London E1 4NS, United Kingdom, and* [¶]*UMR 7141, CNRS and Université Paris-6, Paris F-75005, France*

We investigated the organization of photosystem II (PSII) in agranal bundle sheath thylakoids from a C_4 plant maize. Using blue native/SDS-PAGE and single particle analysis, we show for the first time that PSII in the bundle sheath (BS) chloroplasts exists in a dimeric form and forms light-harvesting complex II (LHCII)·PSII supercomplexes. We also demonstrate that a similar set of photosynthetic membrane complexes exists in mesophyll and agranal BS chloroplasts, including intact LHCI·PSI supercomplexes, PSI monomers, PSII core dimers, PSII monomers devoid of CP43, LHCII trimers, LHCII monomers, ATP synthase, and cytochrome b_6f complex. Fluorescence functional measurements clearly indicate that BS chloroplasts contain PSII complexes that are capable of performing charge separation and are efficiently sensitized by the associated LHCII. We identified a fraction of LHCII present within BS thylakoids that is weakly energetically coupled to the PSII reaction center; however, the majority of BS LHCII is shown to be tightly connected to PSII. Overall, we demonstrate that organization of the photosynthetic apparatus in BS agranal chloroplasts of a model C_4 plant is clearly distinct from that of the stroma lamellae of the C_3 plants. In particular, supramolecular organization of the dimeric LHCII·PSII in the BS thylakoids strongly suggests that PSII in the BS agranal membranes may donate electrons to PSI. We propose that the residual PSII activity may supply electrons to poise cyclic electron flow around PSI and prevent PSI overoxidation, which is essential for the CO_2 fixation in BS cells, and hence, may optimize ATP production within this compartment.

Oxygenic photosynthesis sustains life on Earth. It couples the formation of molecular oxygen with the biosynthesis of carbohydrates, thus providing the ultimate source of biomass, food, and fossil fuels. In the first step of photosynthesis, the solar energy is captured and converted into the energy-rich molecule ATP and the reducing equivalents (in the form of water-derived protons and electrons) used for the conversion of CO_2 into carbohydrates. The light-driven charge separation is conducted by cooperative interaction of photosystem I (PSI)[3] and photosystem II (PSII), two multimeric chlorophyll-binding protein complexes embedded in the thylakoid membranes of cyanobacteria, algae, and plants. The primary charge separation in the reaction centers of PSII and PSI triggers vectorial electron flow from PSII to PSI via the cytochrome (cyt) b_6f complex, also present in the thylakoid membranes, resulting in formation of the electrochemical potential gradient across the thylakoid membrane. In this way, linear electron transport powers the activity of ATP synthase to convert ADP to ATP. Both ATP and NADPH produced in the light-driven redox reactions of photosynthesis are subsequently used for fixation and reduction of CO_2 during the photosynthetic dark reactions of the Calvin-Benson cycle.

Spatial organization of the thylakoid membranes exhibits lateral distribution of the photosynthetic transport complexes. Most of the dimeric photosystem II (PSIIα) is found in the central appressed domains of the grana membranes, where it cooperates with photosystem I (PSIα) in the grana margins to conduct the linear electron flow (1). A pool of PSII, the so-called PSIIβ, also present in the stroma lamellae, donates electrons to the cyclic electron flow under oxidized conditions (1). The PSII core monomers occur predominantly in the stroma lamellae (2), although a recent study showed that some dimeric PSII is also present within this region (3). Under physiological conditions, cyt b_6f is equally distributed within the thylakoid membranes, whereas ATP synthase is localized exclusively in the unstacked stroma lamellae and within the end membranes of the grana stacks (2).

The biochemical photosynthetic pathways are highly conserved among the plant species. Most green plants are C_3 plants, in which the first organic product of photosynthesis is the three-carbon compound phosphoglyceric acid. A second biochemical pathway that allows efficient concentration of CO_2 in leaves exists in C_4 plants, which represent some of the agriculturally most productive crops. This type of plants can sustain higher rates of photosynthesis, thanks to the spatial distribution of the photosynthetic apparatus and the alteration of the leaf

[3] The abbreviations used are: PSI and PSII, photosystem I and II, respectively; BS, bundle sheath; BN, blue native; Chl, chlorophyll; cyt, cytochrome; DDM, β-D-dodecyl maltoside; LHCI and LHCII, light harvesting complex I and II, respectively; MS, mesophyll; DCMU, 3-(3,4-dichloro-phenyl)-1,1-dimethylurea.

structure, both allowing CO_2 to be concentrated around Rubisco (4, 5). In C_4 plants, inorganic carbon is initially fixed in mesophyll (MS) cells into the four-carbon compound oxaloacetic acid. Oxaloacetate is then converted into malate or aspartate, which is transported into bundle sheath (BS) cells, where its decarboxylation provides high concentrations of CO_2 to Rubisco and where the Calvin-Benson cycle occurs (6). Chloroplasts in MS cells contain grana, whereas bundle sheath chloroplasts exhibit various degrees of granal development depending on the plant species, age, and growth conditions (4). In maize, a typical C_4 species of the NADP-malic enzyme subtype, MS chloroplasts are granal at all stages of development, whereas BS counterparts are fully agranal (7, 8).

Although the pathways for carbon assimilation in bundle sheath cells are well established, the exact supramolecular organization of the respective photosynthetic electron transport components has not been fully elucidated. Moreover, the precise biochemical role of PSII in BS chloroplasts remains controversial. Several studies suggested that PSII in maize BS chloroplasts is capable of oxygen evolution, although its activity is very low in comparison with its counterpart in MS chloroplasts (9–14). Other reports suggested that PSII is totally absent in the BS chloroplasts (15, 16) or exhibits no water-splitting activity (16, 17). Moreover, it has been debated whether all of the subunits of PSII, in particular those of the oxygen-evolving complex, are present in the agranal maize chloroplasts (13, 16, 18, 19). It appears that such contradicting reports are due to the differences in the BS isolation procedures and, as a consequence, a degree of intactness of PSII. In addition, it was demonstrated that the level of PSII activity in BS chloroplasts, as well as the presence of the oxygen-evolving complex subunits, depends on the differences in the age of the source leaf tissue, contamination with MS chloroplasts during isolation procedures, and illumination conditions (14, 20, 21). The apparent existence of the D1 degradation/repair cycle in BS chloroplasts and the identification of proteolytic enzymes responsible for these processes in these organelles confirm that PSII indeed plays an important function in the BS agranal membranes (22). Indeed, the active dimeric PSII complexes present in the stroma lamellae of C_3 chloroplasts have been shown to undergo the repair cycle (23, 24), whereby PSII with a damaged D1 reaction center subunit migrates from the grana to the stroma and subsequently undergoes disassembly, repair, and refolding (25).

The higher plant PSII core dimer and its associated light-harvesting antenna, the so-called LHCII·PSII supercomplex, form a basic highly conserved structural unit composed of two LHCII trimers and two copies of the minor Cab (chlorophyll a/b-binding) proteins CP29 and CP26, with each pair symmetrically related by the 2-fold axis of the core dimer (reviewed in Refs. 2 and 26). In C_3 plants, the LHCII·PSII supercomplexes are localized exclusively in the stacked grana regions (2, 27). More complex LHCII·PSII structures exist, in which two or three additional LHCII trimers and two copies of the minor subunit, CP24, associate with the dimeric PSII supercomplex and form complex crystalline arrays within the membranes, depending on the illumination conditions and the species analyzed (2, 3).

Although it has been widely accepted that the structure of membranes in BS chloroplasts seems analogous to the stroma lamellae of C_3 plants, limited direct evidence supporting this notion is available. In this study, we performed comprehensive biochemical and structural characterization of the membrane protein complexes of the granal and agranal maize thylakoids using mild BN-PAGE and two-dimensional SDS-PAGE combined with electron microscopy visualization of the photosynthetic complexes and single particle analyses of negatively stained particles. We demonstrate for the first time that the bundle sheath agranal thylakoid membranes differ significantly from the stroma lamellae of C_3 plants in that PSII in the BS membranes forms the fully functional dimeric supercomplex with its associated LHCII antenna. We propose that the main role of PSII exhibiting residual water splitting activity in BS chloroplasts is to donate electrons from the substrate water molecules into the cyclic electron flow around PSI.

EXPERIMENTAL PROCEDURES

Plant Material and Growth Conditions—Maize (*Zea mays* L. Oleńka, C4 type NADP-malic enzyme) plants were grown in vermiculite in a growth chamber with a 14-h photoperiod and day/night regime at 24/21 °C. Photosynthetic photon flux density was 50, 350, or 800 μmol m^{-2} s^{-1} (for functional measurements). Plants were fertilized with Knop's solution. Leaves were harvested from 3–4-week-old plants.

Chloroplast and Thylakoid Isolation—MS and BS chloroplasts were isolated according to Romanowska *et al.* (21). Isolation procedures were carried out at 4 °C, and 10 mM NaF was added to all buffers. The purity of the BS chloroplasts was determined as 99% (1% residual contamination with MS cells) by assaying the phosphoenolpyruvate carboxylase activity, immunoblotting with anti-phosphoenolpyruvate carboxylase antibodies, determination of Chl *a/b* ratio, and microscopic examination, as described in Ref. 21. For thylakoid preparation, pellets of MS and BS chloroplasts were resuspended in a washing medium containing 50 mM HEPES-NaOH (pH 8.0), 5 mM MgCl$_2$, 10 mM NaCl. After centrifugation at 8,000 $\times$ *g* for 15 min, pellets were resuspended in a washing medium supplemented with 330 mM mannitol. Thylakoid membranes prepared by this procedure were used immediately or snap-frozen in liquid nitrogen and stored at -80 °C until further use. Total chlorophyll content and Chl *a/b* ratio were determined in 80% acetone, according to the method of Arnon (28). PSII activity was assayed spectroscopically by measuring the photoreduction rate of the artificial electron acceptor 2,6-dichlorophenolindophenol, as described in Ref. 14. The photoreduction rates have been determined as 97–108 and 19–22 μmol of 2,6-dichlorophenolindophenol mg^{-1} Chl h^{-1} for MS and BS PSII in freshly isolated thylakoids, respectively. Similar values were obtained for thawed aliquots.

Blue Native-PAGE and Immunodetection—Protein solubilization and BN-PAGE were performed according to Schägger *et al.* (29) and Kügler *et al.* (30) with slight modifications. Thylakoid membranes (50 μg of Chl) were sedimented at 7,000 $\times$ *g* for 5 min at 4 °C and resuspended in a buffer composed of 5 mM EACA, 50 mM imidazole-HCl, pH 7, 50 mM NaCl, 0.5 mM EDTA. Membrane proteins were solubilized by the addition of

n-dodecyl β-ᴅ-maltoside (DDM) to a final concentration of 1% (w/v) (DDM/Chl ratio 20:1) for MS thylakoids and 2% (w/v) (DDM/Chl ratio 40:1) for BS thylakoids (final Chl concentration 0.5 mg/ml). Samples were incubated on ice for 5 min and centrifuged at $15,800 \times g$ for 40 min. The supernatant was supplemented with Coomassie Brilliant Blue solution (100 mᴍ ε-aminocaproic acid (EACA), 30% sucrose) to a final concentration of 10% and loaded directly onto the 4–10% acrylamide, 4–15% sucrose gradient gel. Electrophoresis was carried out using constant 100 V at 4 °C overnight. For separation of protein in the second dimension, the lanes of the BN gels were excised and incubated in the denaturation solution (1% β-mercaptoethanol, 1% SDS) for 15 min at room temperature, followed by 15 min at 50 °C. The strips were briefly rinsed in distilled water and layered onto SDS-polyacrylamide gels (31) with 15% (w/v) acrylamide and 6 ᴍ urea in a separating gel. Electrophoresis was performed using a constant current of 7 mA at 4 °C overnight. Proteins were visualized using Coomassie Brilliant Blue R-250 solution or electrotransferred onto a polyvinylidene difluoride membrane (Millipore) for Western immunodetection. Blots were probed with specific antibodies (anti-PSI L, -Lhca1, -Lhca4, -D2, and -Lhcb1) and visualized by chemiluminescence.

Fluorescence Measurements of Thylakoid Membranes— Room temperature fluorescence measurements were performed with a home-built fluorimeter, using a light source at 590 nm. The fluorescence response was detected in the near IR region. Fluorescence induction kinetics was measured in the presence of 20 μᴍ DCMU to prevent oxidation of the primary quinone acceptor Q_A. Cryogenic fluorescence spectra were recorded at 77 K using a home-built spectrophotometer based on a detecting diode array (AVS-USB 200; Ocean Optics). Samples were loaded into a small metal cuvette (volume ~15 μl), which was directly immersed in the liquid nitrogen bath. Excitation was provided by an LED source (peak at 470 nm, full width at half maximum (FWHM) ~20 nm), which was directed onto the sample through an optical guide. Spectra deconvolution was performed with the MatLab software.

Biochemical Isolation and Characterization of Sucrose Gradient Fractions— 40 mᴍ NaF was added to all the buffers throughout the isolation procedure to inhibit dephosphorylation of phosphoproteins. Thylakoid membranes from MS and BS chloroplasts (0.8 mg/ml Chl) were solubilized with 0.9% DDM and fractionated by centrifugation on continuous sucrose density gradients, as detailed previously (61). Protein analyses were conducted using an SDS-PAGE Tris-Tricine system described by Schägger and von Jagow (32). Protein bands were separated on 12.5% polyacrylamide gels in the presence of 6 ᴍ urea and visualized with Coomassie Brilliant Blue R-250 using standard procedures. Optical absorption spectra were obtained at room temperature using a Shimadzu UV-1601 spectrophotometer with a 2-nm slit size. Steady-state fluorescence emission spectra were measured using a PerkinElmer Life Sciences luminescence spectrometer LS 50 at 77 K and a Chl excitation wavelength of 435 nm.

Electron Microscopy—For the negative staining of protein samples, a concentration of 1–2 μg of Chl/ml was found to be optimal, prior to the addition of 2% (w/v) uranyl acetate via the

droplet technique. Imaging at a magnification of ×30,000, in a low dose mode, with a FEI-Tecnai 12 transmission electron microscope, operating at 120 kV, yielded micrographs of no discernible drift or astigmatism. These were scanned using a Nikon LS9000 CoolScan densitometer at a step size of 6.35 μm, and images were transferred to a networked cluster of Linux-based PC workstations for subsequent single particle image processing.

Image Processing—Micrographs displayed the first minima of their Fourier power spectra in the 19–21 Å range. No correction was made for the contrast transfer function given this minimum value and the presence of negative stain. Data sets were compiled using the automatic particle selection procedures of "boxer," a module of the EMAN software package (see Ref. 33 and references therein). All subsequent image processing was performed using the latest version of the Imagic-5 environment (Image Science GmbH, Berlin). Reference-free alignment followed by multivariate statistical analyses (34) allowed for initial two-dimensional class averages to be identified, which were then iteratively refined, resulting in the final averages shown for each preparation.

RESULTS

Biochemical Characterization of Thylakoids from Mesophyll and Bundle Sheath Chloroplasts—In order to achieve the best resolution of membrane protein complexes during one-dimensional BN-PAGE, we subjected the MS and BS membranes to several rounds of optimization of the detergent/protein ratio (data not shown). Of all of the detergent tested, we selected DDM, since it provided the optimal separation of the membrane protein complexes from both MS and BS thylakoids, especially those in the highest molecular weight range. Fig. 1 shows the BN protein profiles of the solubilized thylakoids from MS (*A*) and BS (*B*) cells. The best resolution of protein complexes on the BN-PAGE gels was achieved using detergent concentrations of 1% (w/v) (DDM/Chl ratio 20:1) and 2% (w/v) (DDM/Chl ratio 40:1) for MS and BS thylakoids, respectively. Under these conditions, 11 main protein bands corresponding to thylakoid membrane complexes from both MS and BS thylakoids were identified (Fig. 1, *top panels* in *A* and *B*). All of these bands were further separated in the second dimension on SDS-PAGE to determine the precise composition of the membrane protein complexes identified on the BN-gels (see Fig. 1, *A* and *B*).

Protein profiles obtained from various plant species using two-dimensional BN/SDS-PAGE are similar due to the high conservation of the subunits of the photosynthetic complexes (24, 30, 35, 36). We therefore identified the components of the BN bands from MS and BS thylakoids by comparison of the apparent molecular weight on BN/SDS-PAGE and by immunodetection using specific antibodies against the subunits of the PSII and PSI cores and the associated LHCII and LHCI antennae (see Fig. 1, *C* and *D*). For both MS and BS thylakoids, complexes of the highest molecular weight on the BN gels were assigned to oligomeric forms of the LHCI·PSI and LHCII·PSII supercomplexes (bands 1–5 in Fig. 1, *A* and *B*), as confirmed by the identification of the PSI core subunits (PSI A/B, PSI F, PSI L, and PSI E), components of the LHCI antenna (Lhca1 and
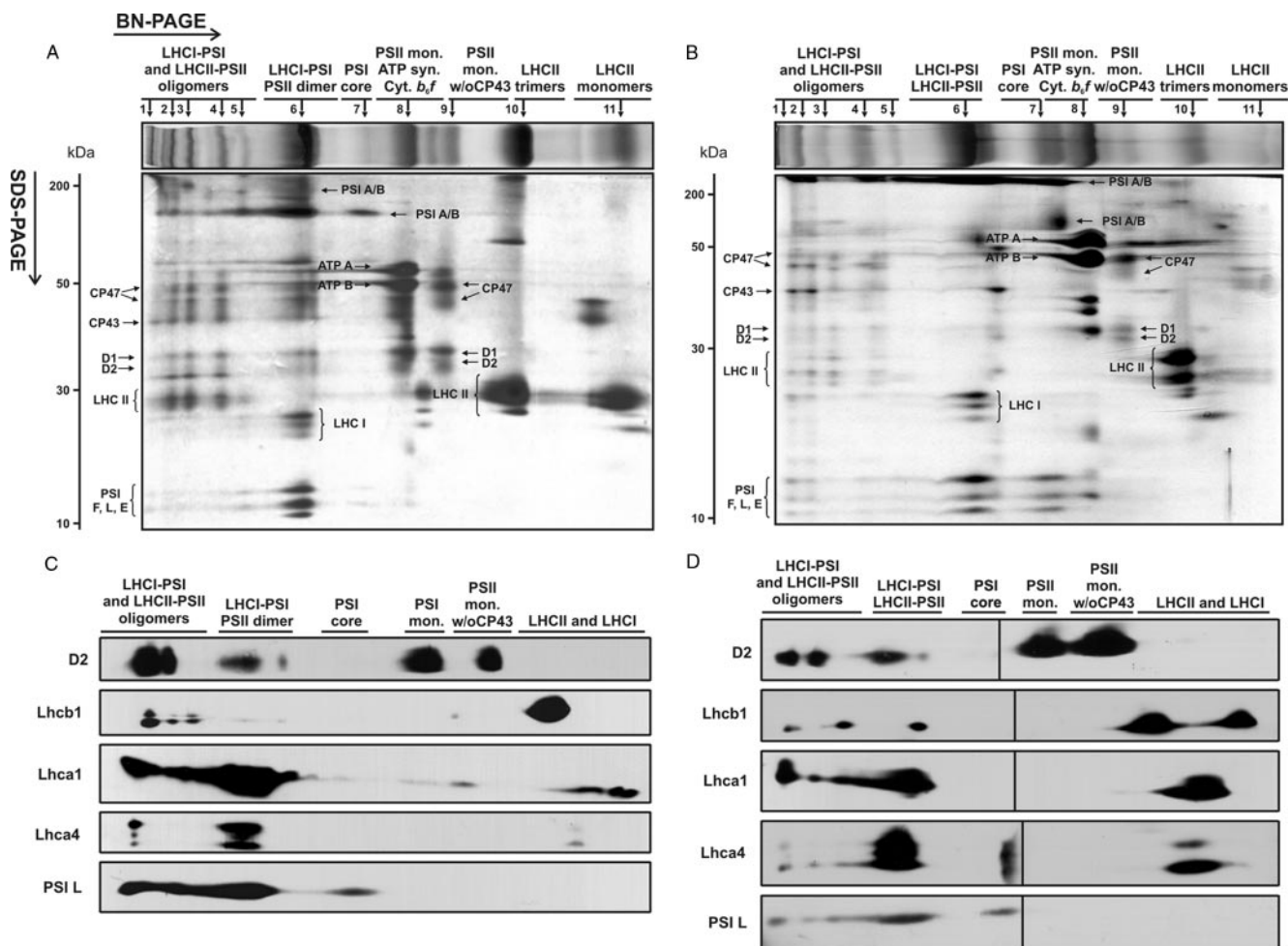
FIGURE 1. **Two-dimensional analysis of protein complexes composition of mesophyll (*A* and *C*) and bundle sheath (*B* and *D*) thylakoids of maize.** Thylakoid protein samples (50 μg of Chl) were solubilized in the presence of 1 and 2% DDM for MS and BS thylakoids, respectively, and loaded onto BN gels (4–10% acrylamide, 4–15% sucrose). For second dimension, lanes were cut out of the BN gels and loaded horizontally onto denaturing SDS-PAGE gels (15% acrylamide, 6 M urea). Protein bands were visualized by Coomassie staining (*A* and *B*) or immunodetected (*C* and *D*) using antibodies against selected subunits of PSI (PSI L, Lhca1, and Lhca4) and PSII (D2 and Lhcb1). Protein bands resolved on BN-PAGE are *numbered above* the BN gel fragments. *w/o CP43*, without CP43. Molecular masses of protein standards (in kDa) are indicated on the *left*. The *black line* in Fig. 1*D* indicates the joining point of the two pieces of the membrane. Note that the immunodetection analysis is not quantitative, since proteins were blotted onto separate membranes.

Lhca4), the PSII core proteins (D1, D2, CP43, and CP47), and the LHCII antenna subunits (Lhcb1). The most intense band 6 from MS thylakoids contained the PSII core dimers and the LHCI·PSI supercomplexes, as confirmed by the detection of the PSI and PSII core subunits as well as the LHCI antenna (Lhca1 and Lhca4). Band 6 from BS thylakoids contained a similar set of PSI and PSII subunits with the additional presence of the LHCII antenna (see immunodetection of Lhcb1 in Fig. 1*D*) and therefore was assigned to the LHCI·PSI and LHCII·PSII super-complexes. Band 7 from both MS and BS membranes corresponded to the PSI core depleted from the LHCI antenna. Band 8 from both MS and BS thylakoids was assigned to the PSII monomer, ATP synthase, and cyt b_6f. Band 9 from both types of membranes contained the PSII monomer devoid of the CP43 inner antenna subunit. Finally, bands 10 and 11 from both MS and BS thylakoids were assigned to the trimeric and monomeric forms of LHCII, respectively, as confirmed by the immunodetection of the Lhcb1 subunit (see Fig. 1, *C* and *D*). In band 11 from both types of membranes, the components of the LHCI antenna were also detected using anti-Lhca1/4 antibodies (see Fig. 1, *C* and *D*).
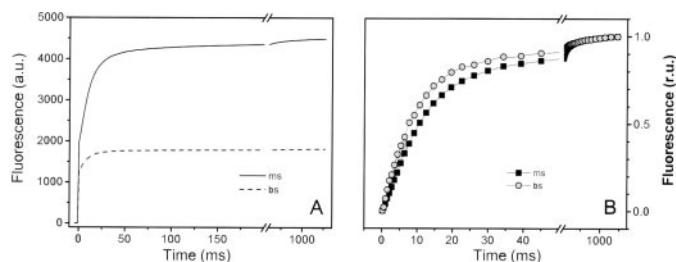

FIGURE 2. **Room temperature fluorescence induction kinetics in meso-phyll and bundle sheath chloroplasts.** Thylakoid protein samples (50 μg of Chl) were exposed to continuous illumination with green light (520 nm) in order to achieve homogeneous absorption. Fluorescence emission was measured in the near infrared region in the presence of the PSII inhibitor DCMU (20 μM). In *B*, the same data as in *A* are presented upon normalization of the variable fluorescence. *a.u.*, absorbance units.

Functional Analysis of Thylakoids from Mesophyll and Bundle Sheath Chloroplasts—Room temperature fluorescence emission measurements of MS and BS thylakoids showed a significantly decreased fluorescence yield in BS thylakoids ($F_v/F_m = 0.33$) compared with MS membranes ($F_v/F_m = 0.65$) (see Fig. 2). Several
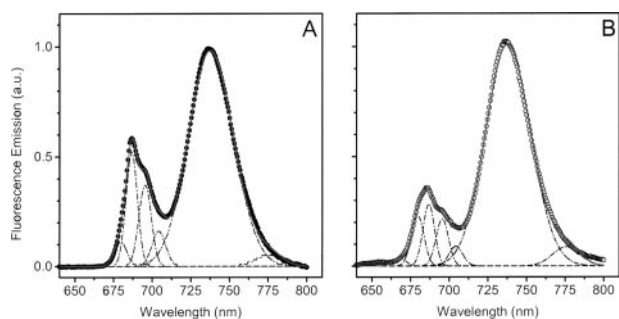
FIGURE 3. **77 K fluorescence emission spectra in mesophyll (*A*) and bundle sheath (*B*) thylakoids.** Thylakoid protein samples (50 μg of Chl) were loaded into a metal cuvette, which was directly immersed in liquid nitrogen. Fluorescence spectra were recorded upon excitation at 470 nm. Emission spectra were deconvoluted with a sum of 5 Gaussian functions (*dotted lines*), and the relative fraction of weakly coupled LHCII was estimated from the ratio between the 680 nm band and the sum of all of the PSII related bands. Peaks were normalized to aid their comparison. *a.u.*, absorbance units.

possibilities can account for this observation, including a decreased PSII/PSI ratio. PSII is responsible for variable fluorescence (F_v) emission at room temperature, whereas PSI contributes only to the constant F_o emission (37). Therefore, a large decrease in the PSII/PSI ratio, as expected in the case of BS chloroplasts, may lead to a decreased F_v/F_m ratio. Alternatively, a weak energetic coupling between LHCII and PSII may decrease the F_v/F_m ratio by increasing the F_o emission component. Indeed, the relatively large pool of LHCII present in BS chloroplasts (14) may not be completely connected to the reduced number of PSII reaction centers. Finally, the occurrence of sustained energy spillover from PSII to PSI may also decrease the fluorescence yield of PSII and thus the F_v/F_m ratio.

In order to distinguish among these hypotheses, we first assessed the actual PSI/PSII ratio in BS and MS chloroplasts by monitoring the electrochromic shift signal, a technique previously used to evaluate the PSI/PSII ratio in freshwater green algae (38). The electrochromic shift signal is triggered by the light-induced electric field that develops across the thylakoid membrane upon charge separation within the reaction centers of the two photosystems (reviewed in Ref. 39). The electric field modifies the spectrum of pigment-containing complexes due to the Stark effect. This can be used to quantitatively assess the reaction center stoichiometry from the amplitude of the fast electrochromic shift signal phase (100 μs), which is proportional to the photochemical activity of both PSI and PSII (38). The relative contribution of PSII can be calculated from the difference between the signal measured in the presence or absence of the PSII inhibitors DCMU and hydroxylamine. When measured in maize chloroplasts, a drop by a factor of 3 ($\sim$0.3) was observed for the PSII component in the BS chloroplast when compared with the MS counterpart ($\sim$1) (not shown). Thus, the reduced PSII/PSI stoichiometry can in principle account for the reduced F_v/F_m ratio measured for the BS membranes.

To verify whether this reduction of PSII amount in the BS thylakoids may also lead to some uncoupling between the PSII reaction center and its LHCII antenna, we measured the fluorescence spectra at cryogenic temperatures. Fig. 3 confirms the reduced PSII content in BS compared with MS membranes, as shown by the diminished ratio between the PSII emission peaks

(685 and 695 nm) and the PSI emission peak (735 nm). Furthermore, the emission spectra indicate the presence of a weakly coupled LHCII pool in BS chloroplasts, as shown by the presence of a clear shoulder in the 680 nm region, where emission from the uncoupled LHCII is expected (40). In order to quantify the extent of weakly coupled LHCII in BS membranes, the 77 K fluorescence spectra were deconvoluted using a sum of Gaussian functions. We found that five Gaussians represented the minimum number to obtain good data fitting, as shown by the match between the measured spectra (data points) and the deconvoluted ones (red lines). Three major bands were observed in both BS and MS membranes: one peaking at 680 nm, a second one at 685 nm, and a third one at 695 nm. A forth band peaking at $\sim$705 nm was also detected, which was previously described (41). Although the relative area of the two major PSII bands (685 and 695 nm) did not change between the BS and MS chloroplasts, there was a significant increase in the 680 nm peak, which represented $\sim$30% of the total PSII emission in BS chloroplast and $\sim$10% in the MS membranes. This suggests that a fraction of the LHCII complexes present within BS thylakoids is weakly coupled to the PSII reaction center.

The weak energetic coupling of the specific fraction of the LHCII complexes was confirmed by measuring fluorescence emission spectra at room temperature. In these conditions, sustained emission in the 675 nm region was seen in BS thylakoids, as expected if they contain some poorly coupled LHCII (data not shown). Nevertheless, it clearly appears that the majority of the LHCII complexes are connected to PSII in BS thylakoids. This is further confirmed by the observation that the rise of fluorescence observed in BS chloroplasts was $\sim$40% faster compared with MS membranes (upon normalization of F_v; see Fig. 3*B*). This indicates that the optical section of the PSII reaction centers was larger in BS compared with MS thylakoids, as expected if most of the LHCII present in the BS membranes was connected to the remaining reaction centers.

An additional conclusion that can be derived from Fig. 3*B* is the lack of sustained spillover from PSII to PSI in BS thylakoids (42). This is indicated by the shape of the fluorescence rise measured in the presence of the PSII inhibitor DCMU, which is clearly sigmoidal. This feature reflects the progressive increase in the light harvesting capacity of a PSII photochemical unit as its PSII neighbors become photochemically inactive due to the reduction of the quinone acceptor Q_A (43, 44). This feature is therefore indicative of an efficient energy transfer between closed and open PSII traps, without any significant competition by energy quenching through PSI photochemistry.

Isolation and Biochemical Characterization of Mesophyll and Bundle Sheath Photosynthetic Complexes—Sucrose gradient fractionation of thylakoid membranes solubilized with 0.9% DDM was performed in order to isolate photosynthetic complexes from MS and BS chloroplasts. Three main Chl-containing bands were obtained for both types of thylakoids (F1, F2, and F3, for MS and BS, respectively). SDS-PAGE of sucrose density fractions isolated from BS thylakoids (see Fig. 4) showed the presence of free LHC proteins in F1, a range of proteins indicative of a mixture of PSII and PSI core subunits in F2 (see identification of PSI A/B, LHCI subunits, CP43, and cyt b_{559}), and the enrichment of the PSI core subunits (PSI A/B) and the
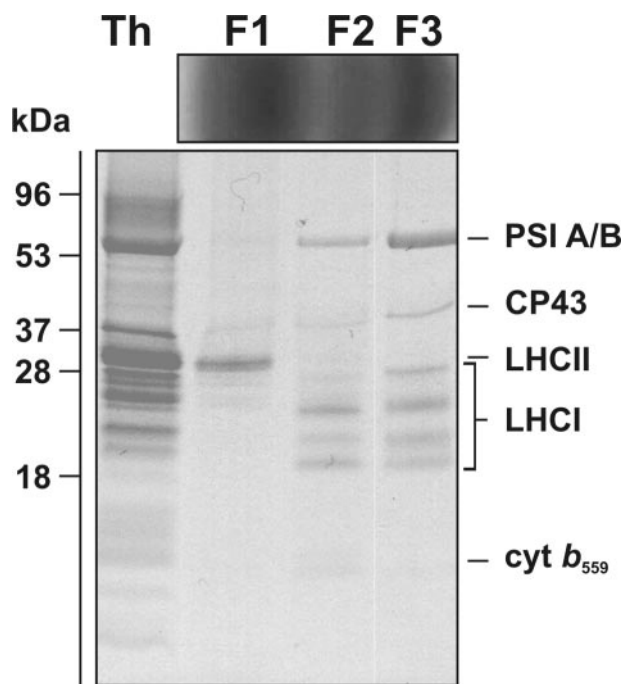
FIGURE 4. **Protein composition of sucrose gradient fractions obtained from solubilized bundle sheath thylakoids.** Sucrose gradient fractions F1–F3 obtained from BS thylakoids are shown *above* the SDS-polyacrylamide gel. Protein markers with their apparent molecular mass (kDa) are indicated on the *left*, *Th*, DDM-solubilized thylakoids from BS cells. Proteins were loaded at 5 μg of Chl, and the resolved bands were stained with Coomassie Brilliant Blue.

four Lhca subunits of the associated LHCI antenna in the F3 fraction from BS thylakoids. In the latter fraction, PSII core subunits, albeit in low amounts, were also identified (see Fig. 4). All of the fractions were also characterized spectroscopically to determine the identity of Chl-containing protein complexes. All fractions were characterized spectroscopically to determine the identity of Chl-containing protein complexes. Room temperature absorption spectroscopy revealed the top fraction (F1) as being free LHC proteins (for both MS and BS) with an absorption maximum at 676 nm and a shoulder at 654 nm due to the presence of Chl *b* (see Fig. 5, *A* and *B*). Fraction F1 was also characterized by having strong absorption in the 450–500 nm range, due to the presence of Chl *b* (peaking at 474 nm) and carotenoids. Fraction 2 (F2 for both MS and BS) (see Fig. 5, *A* and *B*) was characterized by a lack of Chl *b* absorption and a red shift of the long wavelength absorption peak to 678 nm, as compared with F1. The densest fraction (F3 for both BS and MS) showed some Chl *b* absorption at 654 and 474 nm and had a maximum red wavelength peak at 680 nm, consistent with an enrichment of this fraction in the LHCI·PSI supercomplexes.

Each Chl-containing sucrose density band, derived from MS and BS thylakoids, was also characterized by low temperature (77 K) fluorescence, as shown in Fig. 5, *C* and *D*, respectively. The emission profile of fraction F1 (for both MS and BS) peaked at 681 nm, consistent with the presence of free LHC proteins (Fig. 5, *C* and *D*). Fraction F2, from both types of thylakoids, showed an emission spectrum with the main peak of 685 nm and a smaller peak of 730 nm, indicative of a mixture of predominantly PSII (peaking at 685 nm) and a smaller proportion of PSI complexes

partially depleted from the LHCI antenna (see Fig. 5, *C* and *D*). The fluorescence emission spectrum of fraction 3 from BS thylakoids (BS-F3) peaked at 735 nm, indicating the enrichment of LHCI·PSI within this fraction (see Fig. 5*D*). A small peak at 685 nm (less than 10% of the PSI peak) indicated a small proportion of PSII present in the BS-F3 fraction (Fig. 5*D*). In contrast, the densest fraction from MS thylakoids (MS-F3) showed two main fluorescence peaks at 685 and 735 nm, implying the presence of a mixture of PSII and PSI complexes in this fraction (see Fig. 5*C*).

Electron Microscopy—Direct visualization of the protein complexes, in two-dimensional projection, was made possible through the single particle analysis of transmission electron micrographs of negatively stained particles, from the BS sucrose gradient fractions F2 (12 micrographs) and F3 (13 micrographs). After the application of multivariate statistics and subsequent classification of the two data sets, it became apparent that fraction BS-F2 contained two main subpopulations. These were assigned as a typical PSI monomeric core (594 particles), devoid of the LHCI antenna, having dimensions of 150 and 100 Å (see Fig. 6*B*) and a PSII core monomer (330 particles) with dimensions of 145 and 104 Å (Fig. 6*C*). In fraction BS-F3, the most intact populations we assigned to a typical PSII core dimer (502 particles) having dimensions of 220 × 150 Å (see Fig. 6*A*) and the LHCI·PSI supercomplex (103 particles), the latter characterized by a crescent of four Lhca antenna subunits localized asymmetrically on one side of the complex (see Fig. 6*D*). An approximate outline contour of the recent x-ray crystal structure of the pea LHCI·PSI supercomplex (Protein Data Bank code 2o01) (45) was overlaid, to scale, onto the electron microscopy-derived two-dimensional projection maps of the maize PSI core monomers (Fig. 6*B*; PSI monomeric region only) and LHCI·PSI supercomplexes (Fig. 6*D*) to aid orientation of the structural domains within these particles. It is of note that in the crystal structure, the PSI L and PSI H subunits form a characteristic bulge at the tip of the PSI monomer, which is also present along the lower edge of the averaged particles shown in Fig. 6*B*. Another characteristic feature of the pea LHCI·PSI supercomplex x-ray structure is a crescent of four distinct domains corresponding to the Lhca antenna subunits, flanking the side opposite to PSI L/H. Similar features in the projection maps of the maize LHCI·PSI supercomplex and PSI monomer were therefore assigned to PSI L/H and Lhca subunits and used for the approximate alignment and confirmation of the stromal orientation of the projection maps. Notably, neither in fractions BS-F2 nor BS-F3 did we observe larger particles indicative of the putative larger LHCI·PSI supercomplex that might have retained bound mobile LHCII antenna.

DISCUSSION

Features of BS Thylakoids—The spatial organization of thylakoid membranes in BS chloroplasts has been suggested to be analogous to that of the stroma lamellae of C$_3$ plants. Surprisingly, limited data concerning the exact composition of the photosynthetic apparatus in the BS thylakoids are available. Our study presents a comprehensive analysis of the membrane protein complexes of the granal and agranal thylakoids from the typical C$_4$ plant maize. Using blue native PAGE we identified intact LHCI·PSI and LHCII·PSII supercomplexes, PSI
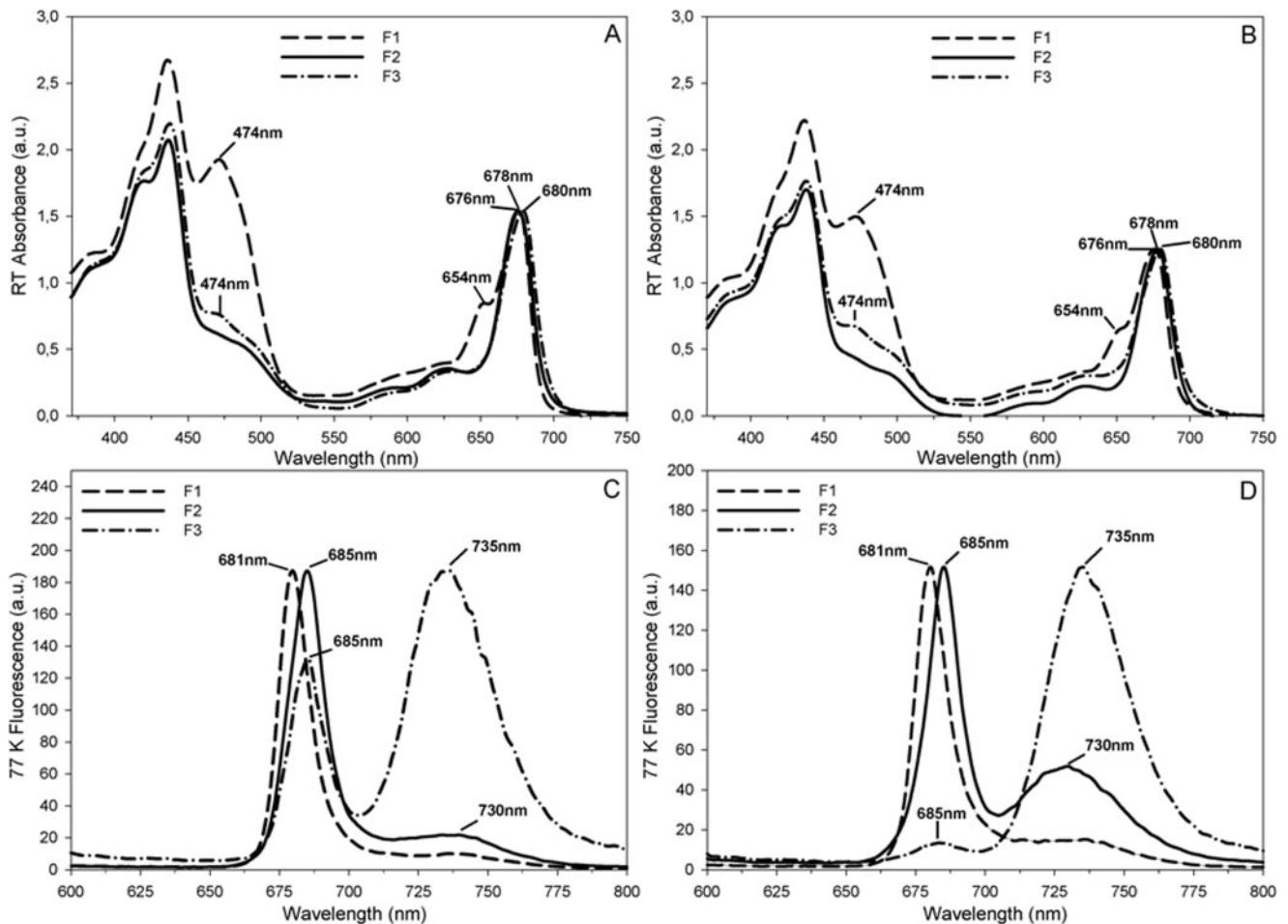
FIGURE 5. **Optical absorbance and fluorescence properties of sucrose gradient fractions obtained from MS (*A* and *C*) and BS (*B* and *D*) thylakoids.** Spectra corresponding to F1 (LHCs), F2 (PSI/PSII), and F3 (LHCI·PSI) fractions are presented as *dashed*, *solid*, and *dotted-dashed lines*, respectively. *A* and *B*, room temperature (*RT*) absorbance spectra. *C* and *D*, fluorescence spectra were recorded at 77 K using excitation at 435 nm. Peaks have been normalized to aid their comparison. *a.u.*, absorbance units.

monomers, PSII core dimers, PSII monomers devoid of CP43, LHCII trimers, LHCII monomers, ATP synthase, and cyt b_6f complex in the MS and BS thylakoid membranes (Fig. 1). As expected, our results of BN- and BN/SDS-PAGE confirm that the protein composition of the C_4 MS membranes is similar to that of the C_3 thylakoids, where all of the complexes listed above are present (24, 30, 35, 36). Our BN/SDS-PAGE identification of the LHCII·PSII supercomplexes in the BS agranal membranes (Fig. 1, *B* and *D*) demonstrates that the BS thylakoids differ in their protein composition from the stroma lamellae of the C_3 plants, in which no dimeric LHCII·PSII supercomplex has been reported to date (3). In addition, the structure of the BS chloroplasts was suggested not to be influenced by the light intensity and was similar in plants grown in full tropical sunlight or under low irradiance (46). In contrast, our recent results have shown that various light growth conditions may alter polypeptide composition of the BS thylakoids of maize (14).

BN-PAGE has been proven a useful approach to investigate the photosynthetic apparatus of higher plants, in particular for the identification of the intact photosynthetic complexes (30). In the present study, we achieved the finest electrophoretic resolution of the thylakoid membrane complexes from the MS and BS chloroplasts of maize by optimization of the procedures described by Kügler *et al.* (30) and Schägger *et al.* (29), in particular by optimizing various detergent concentrations used to solubilize the two types of membranes. In this way, we achieved the best resolution of the protein bands within the highest molecular weight range, including the components of the PSII and PSI reaction centers (see Fig. 1). In agreement with Refs. 24, 30, 35, and 36, we did not observe the oxygen-evolving complex polypeptides, since they are easily detached from PSII during solubilization procedures. Moreover, a pool of PSII monomer lacking CP43 was identified in our study in both types of maize thylakoids (see Fig. 1). A similar complex was reported recently during BN/SDS-PAGE separation of the stroma lamellae of spinach (3). *In vivo* detachment of CP43 occurs during the PSII repair cycle, whereby CP43 undergoes dephosphorylation, which in turn triggers its detachment from the PSII core (47). Interestingly, DDM caused more intensive detachment of CP43 compared with digitonin (data tot shown), in agreement with Heinemeyer *et al.* (35). It cannot be excluded that a subpool of the PSII devoid of CP43 may be a product of the PSII repair cycle, since this pathway has been shown to exist in the BS agranal membranes (22). Additional experiments are required to test this possibility.
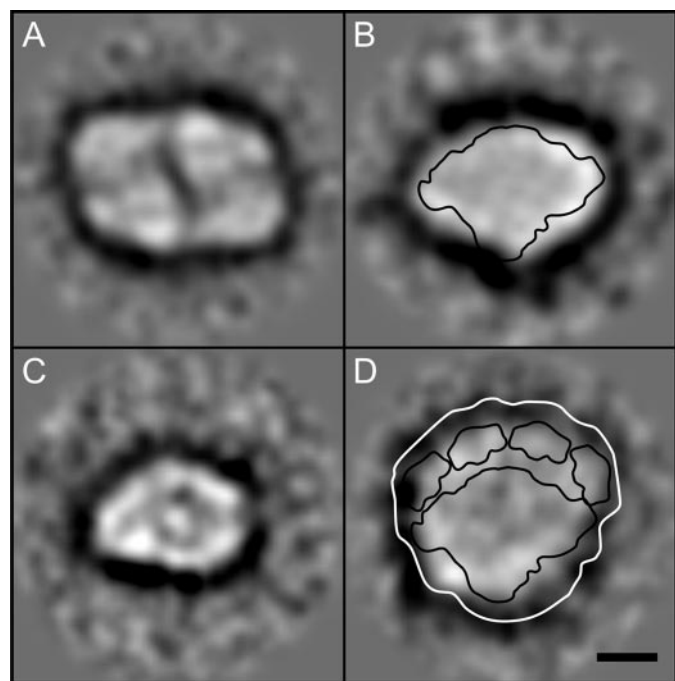
FIGURE 6. Single particle analysis of PSI and PSII complexes obtained from bundle sheath thylakoids. Shown are *top view* class average projections of the PSII dimer (*A*), PSI core (*B*), PSII monomer (*C*), and PSI·LHCI supercomplex (*D*) overlaid with an *outline contour* of a 3.4 Å pea three-dimensional x-ray structure (Protein Data Bank code 2o01) (45). *Scale bar*, 50 Å.

Role of PSII and LHCII in BS Thylakoids—Our functional analysis clearly indicates that BS chloroplasts contain a significant fraction of PSII complexes (about one-third of the PSI centers), which are capable of performing charge separation and are efficiently sensitized by LHCII. Although some of the LHCII complexes present in the BS thylakoids are weakly energetically coupled to the PSII reaction centers, a significant fraction of this light-harvesting complex remains excitonically connected with PSII. Although is possible that the weakly connected LHCII complexes may form aggregates in the membranes, where absorbed energy is largely dissipated nonphotochemically, our fluorescence analysis at room temperature suggests that at least a fraction of LHCII is neither in a quenched state nor connected to the PSII reaction center.

An alternative hypothesis for the functional arrangement of PSII and LHCII in BS chloroplasts is that LHCII remains bound to PSII and may form arrays in the thylakoid membranes facilitating energy transfer between PSII and PSI. This hypothesis is not consistent with the fluorescence kinetic measurements, which clearly indicate lack of sustained spillover and a major association of LHCII to PSII. What is then the function of the LHCII·PSII complexes in the bundle sheath cells? In C_3 plants, photosynthetic protein complexes show heterogeneous lateral distribution along thylakoid membranes. PSII is mostly located in the appressed grana stacks, whereas PSI is concentrated in the nonappressed membranes (*i.e.* the stroma lamellae, the grana margins, and the end membranes). In contrast, the cytochrome b_6f complex is homogeneously distributed (*e.g.* reviewed in Ref. 1). Because of the restricted diffusion of the soluble electron carriers (see review in Ref. 48), it has been proposed that PSII may be able to fuel only those cyt b_6f com-

plexes that are located in the grana. This would elicit an electron flow to the LHCI·PSI supercomplexes that are found at the periphery of the grana and then to ferredoxin. Ultimately, NADPH would be generated at the grana margins and/or grana ends and then consumed, together with ATP, for driving the Benson-Calvin cycle. Although PSI in the stroma lamellae would also reduce ferredoxin, the latter would only access cytochrome complexes, leading to cyclic electron flow (reviewed in Ref. 49).

In C_4 plants, a similar segregation of photosynthetic complexes is observed, which, however, involves a significant decrease of the amount of PSII in a specific compartment (*i.e.* the BS chloroplast). Thus, the segregation between linear and cyclic flow does not occur within the same chloroplast but rather between two separate leaf compartments. The BS chloroplast is essentially involved in the cyclic electron flow leading to the production of ATP that is required, together with the reducing power provided by the mesophyll chloroplasts via the malate shuttle, for CO_2 assimilation (5).

The reduced amount of PSII, which is still present and fully functional in the bundle sheath (*i.e.* in the "cyclic compartment" of maize leaves) may therefore be required to provide reductants as needed for the redox poise control of cyclic flow. Indeed, although in a "perfect" cyclic electron flow system electrons are indefinitely recycled around PSI, when the electron carriers in the stroma become overoxidized, electrons can leak from the cyclic pathway, ultimately leading to a complete inhibition of this process (50). In this sense, the role of PSII would be complementary to that of the NADH-plastoquinone reductase (NDH), which is enriched in the BS chloroplasts (51) and is supposed to inject electrons into the plastoquinone pool, depending on the redox status of the stroma. Alternatively, it has been proposed that ascorbate and malate can cause reduction of stromal donors, which establishes conditions for activation of cyclic electron flow around PSI (52).

Structure of PSII and PSI Complexes in BS Thylakoids—To gain a deeper insight into the structure of maize photosynthetic complexes from the BS agranal membranes, we applied electron microscopy of negatively stained particles, followed by single-particle averaging of the two-dimensional projections. As expected, we confirmed that maize LHCI·PSI supercomplex exists as a monomer with four Lhca antenna subunits associated asymmetrically with the PSI core (Fig. 6*D*). This is in agreement with the recent 3.4 Å x-ray structure of the pea LHCI·PSI supercomplex (45) in which four Lhca subunits of the LHCI complex form a crescent of two dimers that bind asymmetrically to the PSI core. The higher molecular weight oligomeric forms of LHCI·PSI supercomplex identified by our BN-PAGE analysis (Fig. 1) represent artifacts caused by detergent solubilization, as reported previously (53, 54). A relatively high ratio of LHCII/PSII in maize bundle sheath chloroplasts (14, 56) and the significant increase of the functional antenna of PSI within these membranes prompted suggestions that LHCII may act as the antenna for PSI in this compartment (19, 57, 58). We therefore examined whether a fraction of LHCII may transiently associate with the LHCI·PSI supercomplex, leading to an observed increase of the PSI absorption cross-section (data not shown). A similar phenomenon occurs during the process of

state transitions when redistribution of reversibly phosphorylated LHCII between PSII and PSI maintains optimal excitation balance of both photosystems (55, 59). However, we did not detect any projections over and above the classic LHCI·PSI supercomplex, suggesting that in maize, LHCII remains associated with the PSII core. It cannot be excluded, however, that a subfraction of mobile LHCII may transiently associate with PSI but it is displaced following the detergent treatment, as previously reported (60, 61). To explore this possibility, further investigation is required using digitonin solubilization, an approach that has successfully been used to identify a labile LHCII·LHCI·PSI supercomplex in the membranes of a C$_3$ plant, *Arabidopsis thaliana* (60). Alternatively, maize LHCI·PSI may migrate toward PSII to ensure equal excitation energy distribution between both photosystems without the involvement of mobile phospho-LHCII, as recently suggested by Tikkanen *et al.* (62), who reported such a phenomenon during state transitions in the spinach grana margins.

Importantly, our single particle analysis revealed for the first time that PSII forms dimers in addition to monomers in maize BS agranal membranes (Fig. 6*A*), in contrast to the earlier report postulating an exclusively monomeric aggregation state of PSII in maize BS thylakoids (19). The maximum diagonal length of the maize PSII dimer is 200 Å, including a 15-Å detergent shell around this particle. This dimension matches the size of the two-dimensional projection of the spinach PSII core dimer (63). Our single particle analysis did not reveal any LHCII·PSII supercomplexes within sucrose gradient fractions, in contrast to the BN-PAGE results. This apparent discrepancy can be explained by the experimental approach of the sucrose gradient fractionation, which was aimed primarily at the isolation of the intact LHCI·PSI supercomplexes. In this approach, alkaline pH, which is optimal for LHCI·PSI isolation, has been shown to dissociate LHCII from the PSII core (63).

In conclusion, this report demonstrates that the organization of photosynthetic apparatus in BS agranal chloroplasts of a C$_4$ plant species is clearly distinct from that of the stroma lamellae of the C$_3$ plants. The dimeric character of PSII and formation of the LHCII·PSII supercomplex in maize BS agranal thylakoids identified in this study support the idea that PSII plays an important function in this type of membranes, in contrast to the current dogma suggesting functional redundancy of bundle sheath PSII. In particular, the supramolecular organization of the dimeric LHCII·PSII (Figs. 1 and 6) and the existence of the PSII repair cycle (22) in the BS thylakoids strongly suggest that PSII in the BS agranal membranes may donate electrons from the substrate water molecules to a cyclic electron transport around PSI. In C$_4$ plants, ATP is used to drive the C$_4$ cycle, and the requirement for ATP is cell-specific and varies between MS and BS cells. In bundle sheath chloroplast, the cyclic electron flow plays a role in supplying the surplus ATP needed for C$_4$ photosynthesis, and as a consequence, the ATP/NADPH ratio is higher in this type of chloroplasts compared with mesophyll counterparts. This type of electron flow is very sensitive to redox poise and requires activation by a reductant. Residual PSII activity can therefore supply electrons to poise cyclic electron flow, essential for the CO$_2$ fixation in BS cells, and, hence, may optimize ATP production within this compartment.

REFERENCES

1. Albertsson, P.-Å. (2001) *Trends Plant Sci.* **6,** 349–354
2. Dekker, J. P., and Boekema, E. J. (2005) *Biochim. Biophys. Acta* **1706,** 12–39
3. Danielsson, R., Suorsa, M., Paakkarinen, V., Albertsson, P.-Å., Aro, E.-M., Styring, S., and Mamedov, F. (2006) *J. Biol. Chem.* **281,** 14241–14249
4. Hatch, M. D. (1987) *Biochim. Biophys. Acta* **895,** 81–106
5. Leegood, R. C. (2002) *J. Exp. Bot.* **53,** 581–590
6. Sage, R. F. (2004) *New Phytol.* **161,** 341–370
7. Laetsch, W. M. (1971) *Photosynthesis and Photorespiration* (Hatch, M. D., Osmond, C. B., and Slatyer, R. O., eds) pp. 323–349, Wiley-Interscience, New York
8. Yoshimura, Y., Kubota, F., and Ueno, O. (2004) *Planta* **220,** 307–317
9. Mayne, B. C., Edwards, G. E., and Black, P. P. (1970) *Photosynthesis and Photorespiration* (Hatch, M. D., Osmond, C. B., and Slatyer, R. O., eds) pp. 361–371, Wiley-Interscience, New York
10. Bishop, D. G., Andersen, K. S., and Smillie, R. M. (1970) *Photosynthesis and Photorespiration* (Hatch, M. D., Osmond, C. B., and Slatyer, R. O., eds) pp. 323–349, Wiley-Interscience, New York
11. Andersen, K. S., Smillie, R. M., Bishop, D. G., and Bain, J. M. (1972) *Plant Physiol.* **49,** 461–466
12. Chapman, K. S., Berry, J. A., and Hatch, M. D. (1980) *Arch. Biochem. Biophys.* **202,** 330–341
13. Meierhoff, K., and Westhoff, P. (1993) *Planta* **191,** 23–33
14. Drozak, A., and Romanowska, E. (2006) *Biochim. Biophys. Acta* **1757,** 1539–1546
15. Woo, K. C., Anderson, J. M., Boardman, N. K., Downton, W. J. S., Osmond, C. B., and Thorne, S. W. (1970) *Proc. Natl. Acad. Sci. U. S. A.* **67,** 18–25
16. Schuster, G., Ohad, I., Martineau, B., and Taylor, W. C. (1985) *J. Biol. Chem.* **260,** 11866–11873
17. Anderson, J. M., Woo, K. C., and Boardman, N. K. (1971) *Biochim. Biophys. Acta* **245,** 398–408
18. Sheen, J. Y., and Bogorad, L. (1986) *Proc. Natl. Acad. Sci. U. S. A.* **83,** 7811–7815
19. Bassi, R., Marquardt, J., and Lavergne, J. (1995) *Eur. J. Biochem.* **233,** 709–719
20. Oswald, A., Streubel, M., Ljungberg, U., Hermans, J., Eskins, K., and Westhoff, P. (1990) *Eur. J. Biochem.* **190,** 185–194
21. Romanowska, E., Drozak, A., Pokorska, B,. Shiell, B. J., and Michalski, W. P. (2006) *J. Plant Physiol.* **163,** 607–618
22. Pokorska, B., and Romanowska, E. (2007) *Funct. Plant Biol.* **34,** 844–852
23. Mamedov, F., and Styring, S. (2003) *Physiol. Plant.* **119,** 328–336
24. Aro, E. M., Suorsa, M., Rokka, A., Allahverdiyeva, Y., Paakkarinen, V., Saleem, A., Battchikova, N., and Rintamaki, E. (2005) *J. Exp. Bot.* **56,** 347–356
25. Baena-Gonzalez, E., and Aro, E.-M. (2002) *Philos. Trans. R. Soc. Lond.* **357,** 1451–1460
26. Nield, J., and Barber, J. (2006) *Biochim. Biophys. Acta* **1757,** 353–361
27. Kirchhoff, H., Lenhert, S., Büchel, C., Chi, L., and Nield, J. (2008) *Biochemistry* **47,** 431–440
28. Arnon, D. I. (1949) *Plant Physiol.* **24,** 1–15
29. Schägger, H. (2001) *Methods Cell Biol.* **65,** 231–244
30. Kügler, M., Jänsch, L., Kruft, V., Schmitz, U. K., and Braun, H. P. (1997) *Photosyth. Res.* **53,** 35–44
31. Laemlli, U. K. (1970) *Nature* **227,** 680–685
32. Schägger, H., and von Jagow, G. (1987) *Anal. Biochem.* **166,** 368–379
33. Ludtke, S. J., Chen, D. H., Song, J. L., Chuang, D. T., and Chiu, W. (2004) *Structure.* **12,** 1129–1136
34. van Heel, M., Harauz, G., and Orlova, E. V. (1996) *J. Struct. Biol.* **116,** 17–24
35. Heinemeyer, J., Eubel, H., Wehmhöner, D., Jänsch, L., and Braun, H. P. (2004) *Phytochemistry* **65,** 1683–1692

36. Ciambella, C., Roepstorff, P., Aro, E. M., and Zolla, L. (2005) *Proteomics* **5,** 746 –757
37. Duysens, L. M. N., and Sweers, H. E. (1963) in *Studies in Microalgae and Photosynthetic Bacteria* (Japanese Society of Plant Physiologists, eds) pp. 353–372, Tokio Press
38. Joliot, P., and Delosme, R. (1974) *Biochim. Biophys. Acta* **357,** 267–284
39. Witt, H. T. (1979) *Biochim. Biophys. Acta* **505,** 355– 427
40. Butler, W. L., Tredwell, C. J., Malkin, R., and Barber, J. (1979) *Biochim. Biophys. Acta* **545,** 309 –315
41. Ruban, A., and Horton, P. (1992) *Biochim. Biophys. Acta* **1102,** 30 –38
42. Duysens, L. N. M., and Amesz, J. (1962) *Biochim. Biophys. Acta* **64,** 261–278
43. Joliot, P., and Joliot, A. (1964) *C. R. Acad. Sci. Paris* **258,** 4622– 4625
44. Lavergne, J., and Trissl, H.-W. (1995) *Biophys. J.* **65,** 2474 –2492
45. Amunts, A., Drory, O., and Nelson, N. (2007) *Nature* **447,** 58 – 63
46. Downton, W. S. J. (1971) *Photosynthesis and Photorespiration* (Hatch, M. D., Osmond, C. B., and Slatyer, R. O., eds) pp. 3–17, Wiley-Interscience, New York
47. Baena-Gonzalez, E., Barbato, R., and Aro, E.-M. (1999) *Planta* **208,** 196 –204
48. Lavergne, J., and Joliot, P. (1991) *Trends Biochem. Sci.* **16,** 129 –134
49. Johnson, G. N. (2005) *J. Exp. Bot.* **56,** 407– 416
50. Allen, J. F. (2002) *Cell* **110,** 273–276
51. Darie, C. C., De Pascalis, L., Mutschler, B., and Haehnel, W. (2006) *J. Plant Physiol.* **163,** 800 – 808
52. Ivanov, B., Asada, K., Kramer, D. M., and Edwards, G. (2005) *Planta* **220,** 572–581
53. Boekema, E. J., Jensen, P. E., Schlodder, E., van Breemen, J. F. L., van Roon, H., Scheller, H. V., and Dekker, J. P. (2001) *Biochemistry* **40,** 1029 –1036
54. Ben-Shem, A., Frolow, F., and Nelson, N. (2003) *Nature* **426,** 630 – 635
55. Allen, J. F. (2003) *Science* **299,** 1530 –1532
56. Bassi, R., dal Belin Peruffo, A., Barbato, R., and Ghisi, R. (1985) *Eur. J. Biochem.* **146,** 589 –595
57. Bassi, R., and Simpson, D. J. (1986) *Carlsberg Res. Commun.* **51,** 363–370
58. Pfündel, E., Nagel, E., and Meister, A. (1996) *Plant Physiol.* **112,** 1055–1070
59. Kargul, J., and Barber, J. (2008) *FEBS J.* **275,** 1056 –1068
60. Kouril, R., Zygadlo, A., Arteni, A. A., de Wit, C. D., Dekker, J. P., Jensen, P. E., Scheller, H. V., and Boekema, E. J. (2005) *Biochemistry* **44,** 10935–10940
61. Kargul, J., Turkina, M. V., Nield, J., Benson, S., Vener, A. V., and Barber, J. (2005) *FEBS J.* **272,** 4797– 4806
62. Tikkanen, M., Nurmi, M., Suorsa, M., Danielsson, R., Mamedov, F., Styring, S., and Aro, E.-M. (2008) *Biochim. Biophys. Acta* **1777,** 425– 432
63. Hankamer, B., Nield, J., Zheleva, D., Boekema, E., Jansson, S., and Barber, J. (1997) *Eur. J. Biochem.* **243,** 422– 429